THE SEISMOLOGICAL SOCIETY OF AMERICA
400 Evelyn Ave., Suite 201
Albany, CA 94706-1375
(510) 525-5474; FAX (510) 525-7204
www.seismosoc.org

Bulletin of the Seismological Society of America, Vol. 105, No. 2A, pp. 912–927, April 2015, doi: 10.1785/0120140044

Shaking Scenarios from Multiple Source Models Shed Light on the 8 September 1905 M_w 7 Calabria Earthquake (Southern Italy)

by Denis Sandron, Maria Filomena Loreto, Umberto Fracassi, and Lara Tiberi

Abstract The earthquake (M_w 7) that struck western Calabria (southern Italy) on 8 September 1905 profoundly struck a broad region, causing 557 deaths, injuring more than 2000 people, and leaving about 300,000 people homeless. Historical documents also reported a tsunami, although not devastating, for which effects were observed both along the coast and offshore. For all the damage it caused, this event was much studied but not fully explained. Literature source models for the 1905 earthquake are numerous and diverse, in fault geometry, location, and even associated magnitude. They also differ in nature, because these solutions are either field-based or derived from tsunami modeling and macroseismic data inversion. Above all, few or none of the previously published source models appear to be fully compatible with the damage pattern caused by this earthquake.

To contribute to the identification of the seismogenic source of this destructive event, we computed a series of ground-shaking scenarios based on the different fault-source models that various authors associated with this event. The only documented data available that are suitable for our comparative purposes are the macroseismic intensities associated with localities affected by the event. Our results show that shaking scenarios for two out of seven literature source models are compatible with the damage distribution caused by the 1905 earthquake. The different parameters and boundary conditions constraining these two solutions suggest that either seismogenic source should include further complexities. Alternatively, because these two sources are antithetic and partially form a graben, they might have kinematically interacted, if passively, on 8 September 1905. Also, our critical analysis attempts to take site effects into account, at least qualitatively, allowing a more robust evaluation of damage distribution against numerical models.

Introduction

The instrumental era of seismology facilitates reliable detection and location of earthquakes and estimation of their magnitude based on recordings. This was especially true for the last few decades of the twentieth century, when density and geometry of seismic networks dramatically improved. On the other hand, earthquake location can prove challenging when dealing with historical events, including the early-twentieth-century event that is the subject of this article. For preinstrumental earthquakes, epicentral location and magnitude estimates can be doubtful (Bakun and Wentworth, 1997; Gasperini *et al.*, 2010). Such uncertainties can be increased by the lack of adequate seismological recordings and, at times, of other tools of investigation (e.g., geological information). Also, high degree intensities are sometimes biased by local amplification due to site effects (e.g., Castro *et al.*, 1996; Gallipoli, 1999; Mucciarelli *et al.*, 2000; Cara *et al.*, 2005). Estimating epicentral location and magnitude can be further limited for damaging earthquakes that occurred on offshore faults (Fracassi *et al.*, 2012). This circumstance reduces the available macroseismic data points and/or access to geophysical and geological data, which is critical to identify active tectonic features associated with the given earthquake.

The uncertainties intrinsic to historical events, combined with the lack of complete datasets, including both on-land effects and submarine evidence, may lead to numerous solutions for a single earthquake that are often incompatible with each other. Consequently, the search for the causative source of offshore earthquakes poses several challenges and requires a multidisciplinary approach. With this respect, seismological modeling of macroseismic data may provide an essential contribution to discriminating among numerous solutions. On the night of 8 September 1905, a large earthquake ($M_w \sim 7$) struck the Calabria region (southern Italy), causing 557 deaths, injuring more than 2000 people, and leaving about 300,000 people homeless. It triggered a tsunami that was observed along the coast and at sea (Baratta, 1906; Tinti and Maramai, 1996; Guidoboni *et al.*,

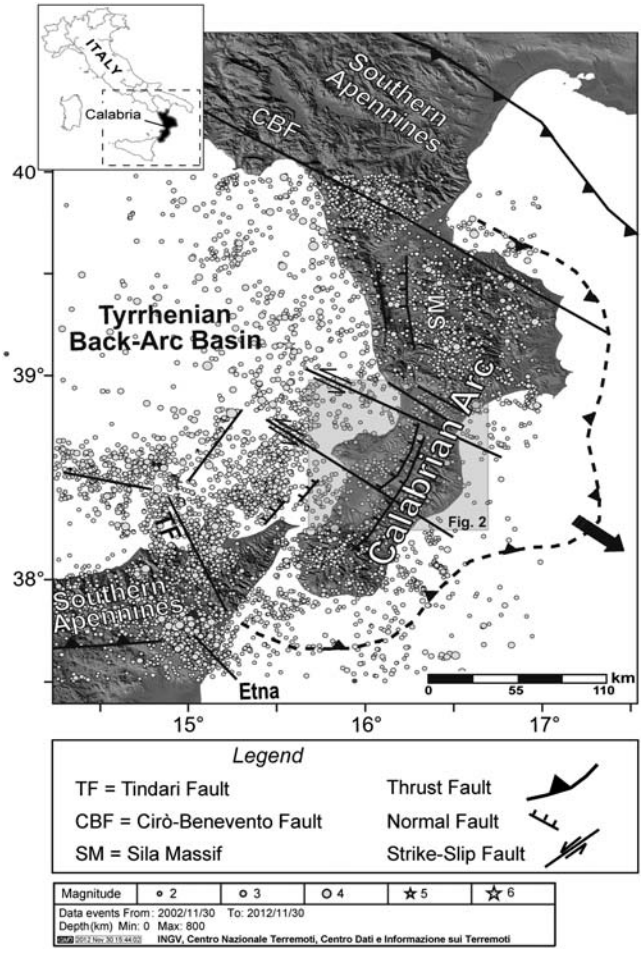

Figure 1. The Calabrian arc system and instrumental seismicity from 30 November 2002 to 30 November 2012 (ISIDe Working Group, 2010).

2007, see Data and Resources; Guidoboni and Ebel, 2009; National Geophysical Data Center/World Data Service, 2012). This destructive event seems to be a typical case study, including virtually all the uncertainties mentioned above (Tiberti *et al.*, 2006), such as (1) lack of a unique epicentral location, (2) lack of a unique seismogenic source solution, and (3) inclusion of a wide range of magnitude estimates. Accordingly, several authors proposed different solutions for this event using different data and analytical methods.

To date, seven seismogenic source models, located either offshore or onshore and within or near the Sant'Eufemia Gulf (southeast Tyrrhenian Sea), have been published. For this work, we modeled the ground-motion resulting from each source to identify the model that could best explain the damage field caused by the 1905 Calabria earthquake. We also compared our results with residuals between observed and predicted intensities to explore possible source complexities.

Geodynamic Setting

The Sant'Eufemia Gulf lies between the Calabrian arc and the southeast Tyrrhenian basin (Fig. 1), which is the Neogene back-arc basin of the Apennines subduction system (Patacca *et al.*, 1990, 1993; Patacca and Scandone, 2004, and references therein). The Calabrian arc (Fig. 1) is an independent, continental block that bridges the northwest–southeast-trending southern Apennines (to the north) with the approximately east–west-trending Apennines in Sicily (to the south) (Bonardi *et al.*, 2001). Its arcuate shape can be attributed to the diachronous collision of the northern and southern Apennine chain with their respective foreland domains (Malinverno and Ryan, 1986; Dewey *et al.*, 1989; Van Dijk *et al.*, 2000). The rapid southeastward migration of the Calabrian arc and the abundant seismicity recorded at different depths (Fig. 1) support the hypothesis that subduction of the oceanic crust is still active beneath the Calabrian block and is laterally constrained by two main tear faults, the Tindari fault (to the south) and the likely Cirò-Benevento fault (to the north; Fig. 1; Van Dijk and Scheepers, 1995; Faccenna *et al.*, 2001, 2014; Rosenbaum *et al.*, 2008; Orecchio *et al.*, 2014). Collision and subduction processes could also be responsible for the intense fragmentation of the Calabrian arc in blocks bounded by the northwest–southeast-striking shear zones (Fig. 1; Knott and Turco, 1991; Van Dijk, 1991, 1992; Barone *et al.*, 2008; Del Ben *et al.*, 2008). Since middle Pleistocene times, the Calabrian arc experienced a rapid uplift up to ~1 mm/yr (Westaway, 1993; Bordoni and Valensise, 1998; Tortorici *et al.*, 2003), in part accommodated by major northeast–southwest-trending normal faults (Ghisetti, 1984; Monaco and Tortorici, 2000; Catalano *et al.*, 2003; Pizzino *et al.*, 2004).

Review of the 8 September 1905 Calabria Earthquake

The 1905 earthquake occurred at the very beginning of the instrumental era and is one of the most debated destructive events of the Italian catalog. Its epicenter (see white stars in Fig. 2) is located offshore by Riuscetti and Schick (1975), Camassi and Stucchi (1997), Michelini *et al.* (2006), and based on recent macroseismic studies by Rovida *et al.* (2011). However, Rizzo (1906), Boschi *et al.* (2000), and Guidoboni *et al.* (2007, see Data and Resources) all located this event inland. With the exception of selected historical seismograms (Michelini *et al.*, 2006), the only available data are the macroseismic intensities. Depending on the available data and methods applied, magnitude estimates in the literature range widely. Instrumental ones span from M_w 7.0 (Martini and Scarpa, 1982), to M_w 7.3 (Mulargia *et al.*, 1984), to M_w 7.5 (Michelini *et al.*, 2006), with the latter based on a complete recovery and revision of historical recordings (data from Rizzo, 1906; Schweitzer and Lee, 2003). On the other hand, macroseismic estimates range from M_w 6.2 (Westaway, 1992) and 6.7 (Guidoboni *et al.*, 2007; see Data and Resources) to M_w 7.0 (Gruppo di Lavoro CPTI, 2004; Rovida *et al.*, 2011) and M_w 7.1 (Postpischl, 1985).

During the past 15 years, numerous authors proposed various faults and seismogenic sources responsible for this event, based on available data and seismological models

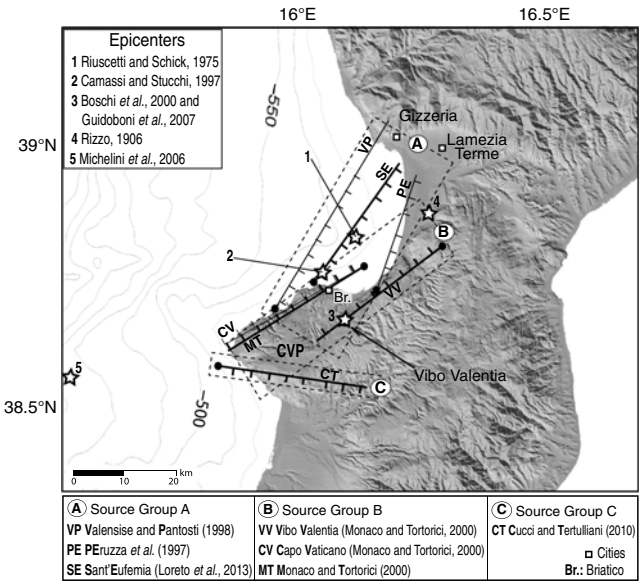

Figure 2. Locations of faults either identified or hypothesized by several authors as possible seismogenic sources of the 1905 earthquake. The legend lists the IDs of models and respective references broken down in groups. CVP, Capo Vaticano promontory. The stars indicate the 1905 epicentral locations proposed by the authors listed in upper left inset.

(Table 1). In particular, Peruzza *et al.* (1997) hypothesized an east-dipping normal fault subparallel to the extensional axis of the Calabrian arc (PE in Fig. 2). Monaco and Tortorici (2000) proposed a northwest-dipping, northeast–southwest-oriented normal fault called the Capo Vaticano fault (MT in Fig. 2). Valensise and Pantosti (2001) proposed a southeast-dipping, northeast-striking normal fault near the edge of the Sant'Eufemia Gulf (VP in Fig. 2). Piatanesi and Tinti (2002) parameterized the Capo Vaticano and the Vibo Valentia faults (Monaco and Tortorici, 2000), two northwest-dipping, northeast–southwest-striking normal faults (CV and VV in Fig. 2). Cucci and Tertulliani (2006, 2010) suggested the Coccorino fault, a south-dipping, west-northwest–east-southeast-oriented normal fault in the southern Capo Vaticano Promontory (CT in Fig. 2). Finally, Loreto *et al.* (2013) proposed a southeast-dipping normal fault, N31°-trending, identified offshore close to the shoreline, between the localities of Briatico and Lamezia Terme (SE in Fig. 2). For an overview of seismogenesis in western Calabria and its geometric relationship with the sources mentioned above, the reader may refer to Basili *et al.* (2008) and the Database of Individual Seismogenic Sources (DISS) Working Group (2010, and references therein).

Source Modeling Technique

In a deterministic approach like ours, a single scenario earthquake is commonly used to show the amount of ground shaking at various sites caused by a nearby earthquake of a given magnitude. Critical input for modeling is fault geometry characterization and parameterization, including strike, dip, and rake (Table 1). We modeled each fault as a rectangular plane. Where available, we obtained geometric parameters from the literature (see PE, SE, CV, and VV in Table 1). Otherwise, we assumed parameters from mapped fault traces and associated data (VP, MT, and CT in Table 1), in which case we derived fault dimensions using empirical relationships by Kanamori and Anderson (1975) and Wells and Coppersmith (1994). The slip vector describes the fracture process on the fault plane as a function of coordinates and rupturing time. To reproduce the fault-plane complexity (Sandron *et al.*, 2008; Tiberi *et al.*, 2014), we assumed *a priori* (1) uniform seismic moment (M_0) distribution on the source plane, smoothed on the margins (U-case); (2) M_0 distribution concentrated in the restricted area surrounding the centroid of the source plane (single asperity; 1A-case; Fig. 3a), with slip vector higher in modulus than its average (Sommerville *et al.*, 1999); and (3) M_0 distribution concentrated in two asperities shifted along strike in the middle of the source plane (2A-case; Fig. 3b), modeled using the k^2 law (Herrero and Bernard, 1994). Rupture propagation velocity V_r is assumed to be constant (equal to 70% of the shear-wave velocity) and not dependent on seismic moment

Table 1
Parameters for the Source Models Causative of the 8 September 1905 Earthquake Available in the Literature

ID*	*R* (Latitude, Longitude)	*H* (km)	M_w	Strike (°)	Dip (°)	Rake (°)	Length (km)	Width (km)
PE	38.71° N, 16.17° E	1	6.6	23	30	270	22	14
VP	38.68° N, 15.95° E	1	7.1	36	30	270	40	20
SE	38.73° N, 16.06° E	0.5	6.8	31	38	270	25	14
MT	38.77° N, 16.15° E	0	6.8	243	30	270	30	16
CV	38.77° N, 16.15° E	0	7	245	80	270	30	20
VV	38.80° N, 16.31° E	0	7	238	80	270	30	20
CT	38.57° N, 15.80° E	5	6.7	100	60	270	29	20

R, reference position (source upper left corner); *H*, source top depth; *L*, source length; *W*, source width; M_w, moment magnitude.

*PE, Peruzza *et al.* (1997); VP, Valensise and Pantosti (2001); SE, Sant'Eufemia (Loreto *et al.* (2013); MT, Monaco and Tortorici (2000); CV, Capo Vaticano (Monaco and Tortorici, 2000); VV, Vibo Valentia (Monaco and Tortorici, 2000); CT, Cucci and Tertulliani (2010).

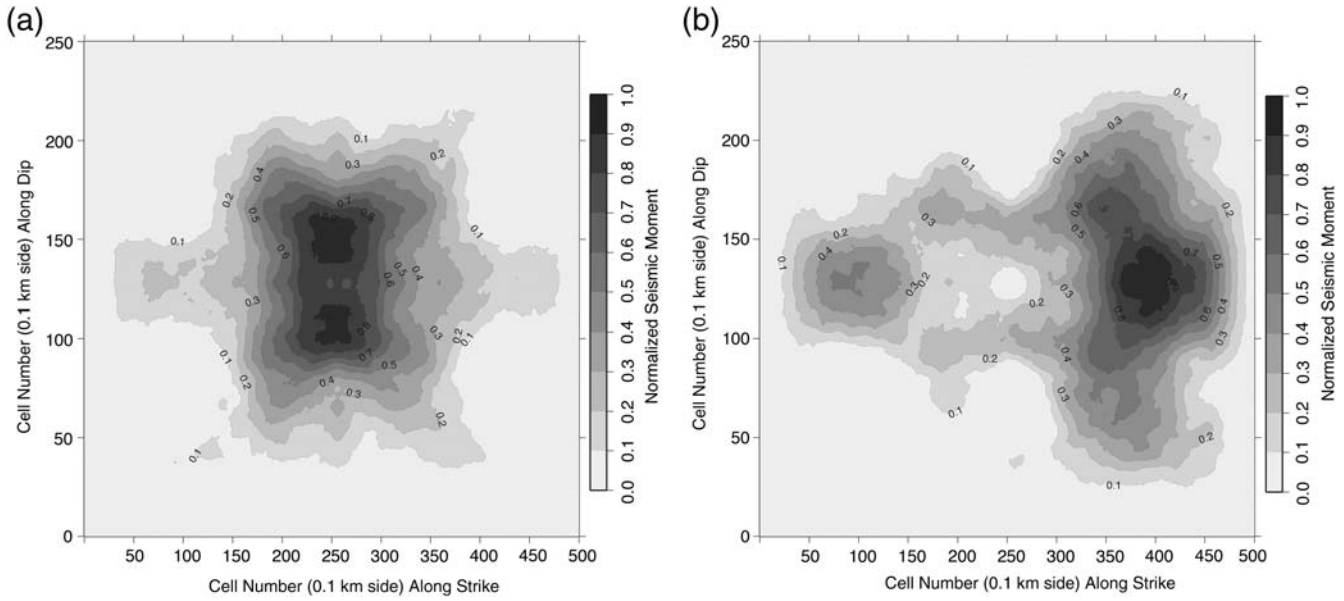

Figure 3. Normalized seismic moment distribution on the source plane, according to the k^2 law (Herrero and Bernard, 1994), using (a) a single asperity located at the center of the source plane, and (b) two asperities shifted along the middle of the source plane.

(Das and Suhadolc, 1996). The rupture can propagate bilaterally from the centroid of the source plane or from an arbitrary nucleation point. Once a structural model of the area of interest is adopted, synthetic seismograms are calculated either over a set of sites or on a grid of receivers equally distributed around the fault region (Costa *et al.*, 1993; Fitzko *et al.*, 2004; Sandron *et al.*, 2008; Tiberi *et al.*, 2014). We computed synthetic seismograms using the modal summation method (Panza, 1985; Panza and Suhadolc, 1987; Florsch *et al.*, 1991; Panza *et al.*, 2001), for a maximum frequency content of 1 Hz and for extended sources (Saraò *et al.*, 1998). We then employed the resulting maximum ground acceleration, velocity, and displacement values to develop contour maps.

Concerning the 8 September 1905 Calabria earthquake, we modeled seven seismogenic source models (Fig. 2; see parameters in Table 1); for each source, we introduced a ± 0.4 M_w uncertainty, with M_w 7 being the mean value from the literature data reported above (0.37 is the uncertainty reported by Rovida *et al.*, 2011, for this event). For each model, we considered the three types of M_0 distributions, adopting a bilateral rupture propagation, with a nucleation point located at the center of the source plane.

Macroseismic Dataset of the 8 September 1905 Calabria Earthquake

The damage field caused by the 1905 event exhibits an extremely uneven intensity distribution (Fig. 4; data from the Italian macroseismic database DBMI11, Locati *et al.*, 2011). Despite such irregularities, it is possible to recognize a general trend of the macroseismic pattern. Although the epicenter of the earthquake is located in the Sant'Eufemia Gulf, the damage distribution is characterized by high values recorded near the villages of Triparni and Pargheria to the southwest and Martinaro and Gizzeria to the northeast, defining a north-northeast–south-southwest trend of higher values.

The damage pattern in Figure 4 provides a benchmark to validate any kind of simulated ground motion. To obtain a quantitative estimate, and following the approach by Suhadolc *et al.* (2004), we computed synthetic seismograms for each site where macroseismic intensities were reported (421 localities). Afterward, we converted peak ground velocity (PGV) values into Mercalli–Cancani–Sieberg (MCS; Sieberg, 1930) intensities, using the empirical relationship by Faccioli and Cauzzi (2006). We preferred this formulation over the more recent ones proposed by Faenza and Michelini (2010), because the former correlation is based on a critical review of selected and documented observational and instrumental datasets, mostly from Italian earthquakes, apparently more robust and suited to the Italian territory.

Generally, low-intensity degrees correlate fairly well with both peak ground acceleration (PGA) and PGV, whereas PGV correlates better with high intensities (Wald *et al.*, 1999; Boatwright *et al.*, 2001; Bommer and Alarcon, 2006). Moderate damage (VI–VII MCS) is usually reported for rigid structures (masonry walls, chimneys, etc.), because these tend to be sensitive to high-frequency ground motion (acceleration). Strong damage also occurs on elastic structures, for which damage is proportional to ground velocity instead of acceleration (Wald *et al.*, 1999). We decided to focus on PGV because (1) the 1905 event is characterized by high intensities and (2) there is a direct relation between velocity and kinetic energy that relates well with damage (Kaka and Atkinson, 2004).

Macroseismic intensities are determined by the degree of damage to people and the man-made environment as a result of ground shaking. Consequently, it cannot simply

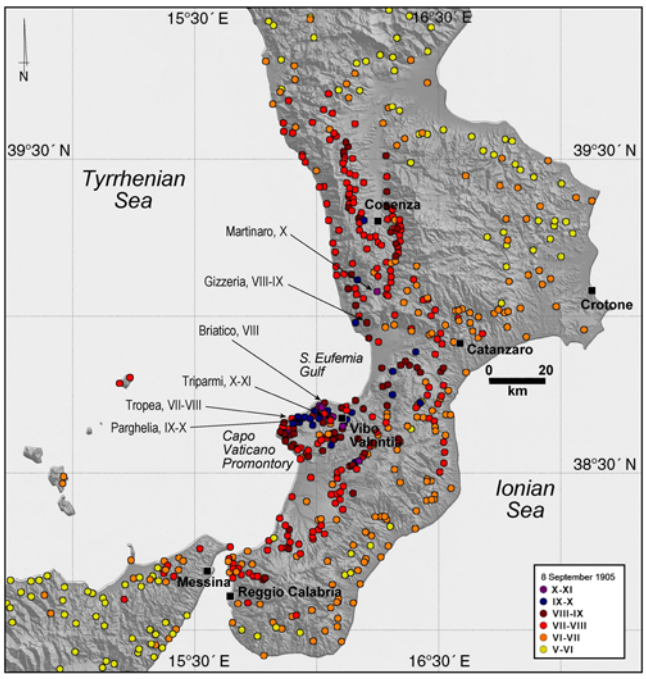

Figure 4. Macroseismic intensities of the 1905 earthquake (data from Locati *et al.*, 2011). Specific localities with respective Mercalli–Cancani–Sieberg (MCS) intensities are identified. The color version of this figure is available only in the electronic edition.

be compared with acceleration or velocity values, either instrumentally recorded or numerically simulated. Although it is largely accepted that there is a likely relationship between intensity and $\log_{10}$ of either PGA and/or PGV (Wald *et al.*, 1999; Atkinson, 2001; Boatwright *et al.*, 2001; Yih-Min *et al.*, 2003), the commonly used empirical regressions are mainly statistical. Table 1 in Gomez Capera *et al.* (2007) shows a summary of PGA and PGV intensity relations in the international context proposed in the literature. The main problem is that the available database is somewhat inadequate, especially concerning instrumental data. The comparison between different relationships reveals the range of variability of estimated intensities derived from the same acceleration or velocity values (Sandron and Loreto, 2012).

Moreover, the PGA and PGV intensity comparison becomes more complex if we take into account site effects that may have influenced the resulting intensity values for given localities, depending on their physical location (i.e., whether on hard rock, soft soil, etc.). To improve this analysis, we considered the statistical distribution (Table 2) of the intensity data against the lithological classification of the Calabria region by Di Capua, Lanzo, *et al.* (2011) and Di Capua, Peppoloni, *et al.* (2011), in compliance with the Italian construction code (Norme Tecniche per le Costruzioni [NTC], 2008). Sites on soil type D (loose, coarse, and fine deposits) (Fig. 5d; Table 2) are few (23 sites) and are located mostly away from the mesoseismal area, except for Nicotera Marina (intensity I = VIII) to the south, Bivona (I = VIII–IX), and Vibo Valentia Marina (I = VII) to the north of the Capo Vaticano promontory. Further sites lie either on the Messina Straits or along the Ionian coast, together with 46 sites mainly on soil type A (bedrock). A small cluster of localities on soil type A lies in the area bearing the highest damage (Fig. 5a), including San Leo and Favelloni (I = X), Briatico, Corridoni, and Pannaconi (I = IX–X), Scicconi (I = VIII–IX), and Cessaniti (I = VIII). A large number of sites (87) on soil type C (tight, coarse, and fine deposits) are concentrated in the mesoseismal area, including Zammarù, with I = XI (Fig. 5c; Table 2). All the remaining localities (264) lie on soil type B (soft rocks; stiff deposits).

Results

We broke down the ground-motion models, computed using the seven source models as input (Fig. 2), into three main groups: (1) group A, including SE, PE, and VP, which strike in a range between 21° and 36° N and are located at different longitudes within the Sant'Eufemia Gulf; (2) group B, including MT and CV, located on the northern shore of the Capo Vaticano promontory (strike 243° and 245° N, respectively), and although shifted slightly to the northeast and more inland, VV (strike 238° N); and (3) group C, including the only 100° N-striking CT fault model, located on the southern flank of the promontory.

Figures 6–8 show the contour maps of PGV derived from synthetic seismograms calculated on the 421 intensity points. We treated the seven input fault models using a uniform propagation (U-case), one asperity (1A-case), and two asperities (2A-case). We contoured MCS values using the natural neighbor bivariate interpolation (Sirovich *et al.*, 2002).

Table 2
Statistical Distribution of the Mercalli–Cancani–Sieberg (MCS) Intensity Dataset According to the Lithological Classification of the Sites after Di Capua, Lanzo, *et al.* (2011) and Di Capua, Peppoloni, *et al.* (2011)

Soil Types	Intensity (I)							Total Sites
	V	VI	VII	VIII	IX	X	XI	
Soil type A (V_S > 800 m/s)	2	4	21	11	3	5	0	46
Soil type B (360 < V_S < 800 m/s)	4	13	115	93	28	11	0	264
Soil type C (180 < V < 360 m/s)	0	1	16	48	14	7	1	87
Soil type D (V_S < 180 m/s)	0	2	12	8	1	0	0	23
Total for intensity level	6	20	164	160	46	23	1	420

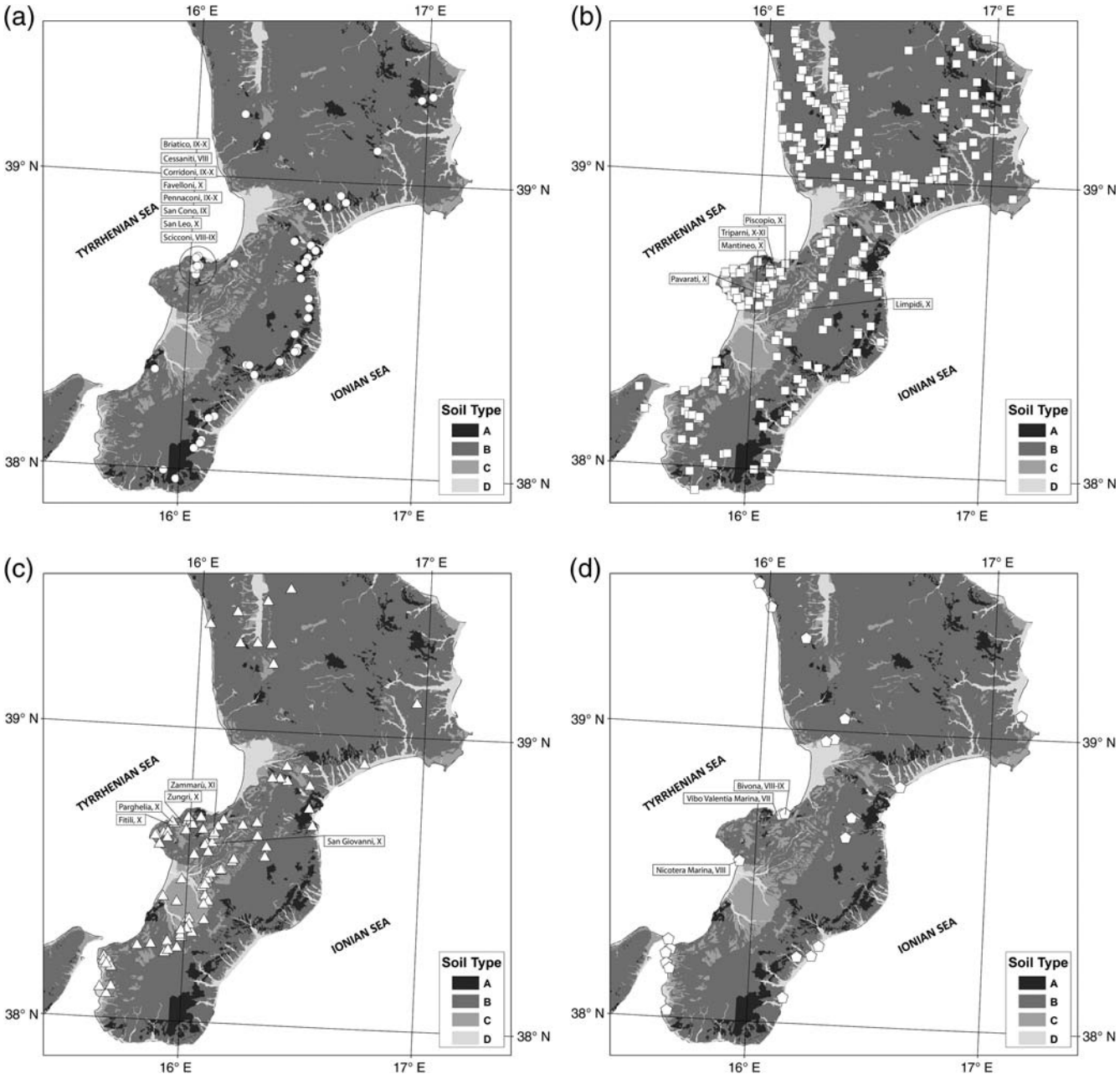

Figure 5. Macroseismic intensity sites located on (a) soil type A (bedrock), (b) soil type B (soft rocks, stiff deposits), (c) soil type C (tight, coarse, and fine deposits), and (d) soil type D (loose, coarse, and fine deposits), according to the lithological classification by Di Capua, Lanzo, *et al.* (2011) and Di Capua, Peppoloni, *et al.* (2011).

Resulting contours include 211 intermediate degrees plotted as half degrees (Pettenati *et al.*, 2011).

Figure 6 shows the PGV distribution for the seven models assuming a uniform M_0 distribution on the fault source. Models in Group A are characterized by a higher PGV distribution trending north-northeast–south-southwest. Model PE shows very low velocity values with a relative maximum of 83 cm/s near the city of Vibo Valentia (IX MCS). SE and VP models show a PGV trend comparable with the MCS pattern, including two relative maxima; one close to the city of Briatico (176 cm/s vs. IX MCS) to the south, and the other one close to Gizzeria (115 cm/s versus VII–IX MCS) to the north (Fig. 6). Models in Group B show an uneven distribution pattern of high PGV values (Fig. 6). Because of the absolute maximum registered at Triparni (343 cm/s versus X MCS) and to a second relative maximum northeast of Vibo Valentia, VV is the model showing a PGV pattern most compatible with intensities distribution. Model CV also shows a PGV trend that well fits the intensity pattern, although without outstanding maximum PGV values (Fig. 6). Model MT shows only one maximum in Parghelia (244 cm/s versus X MCS; Fig. 4). The CT model, in Group C (Fig. 6), shows very

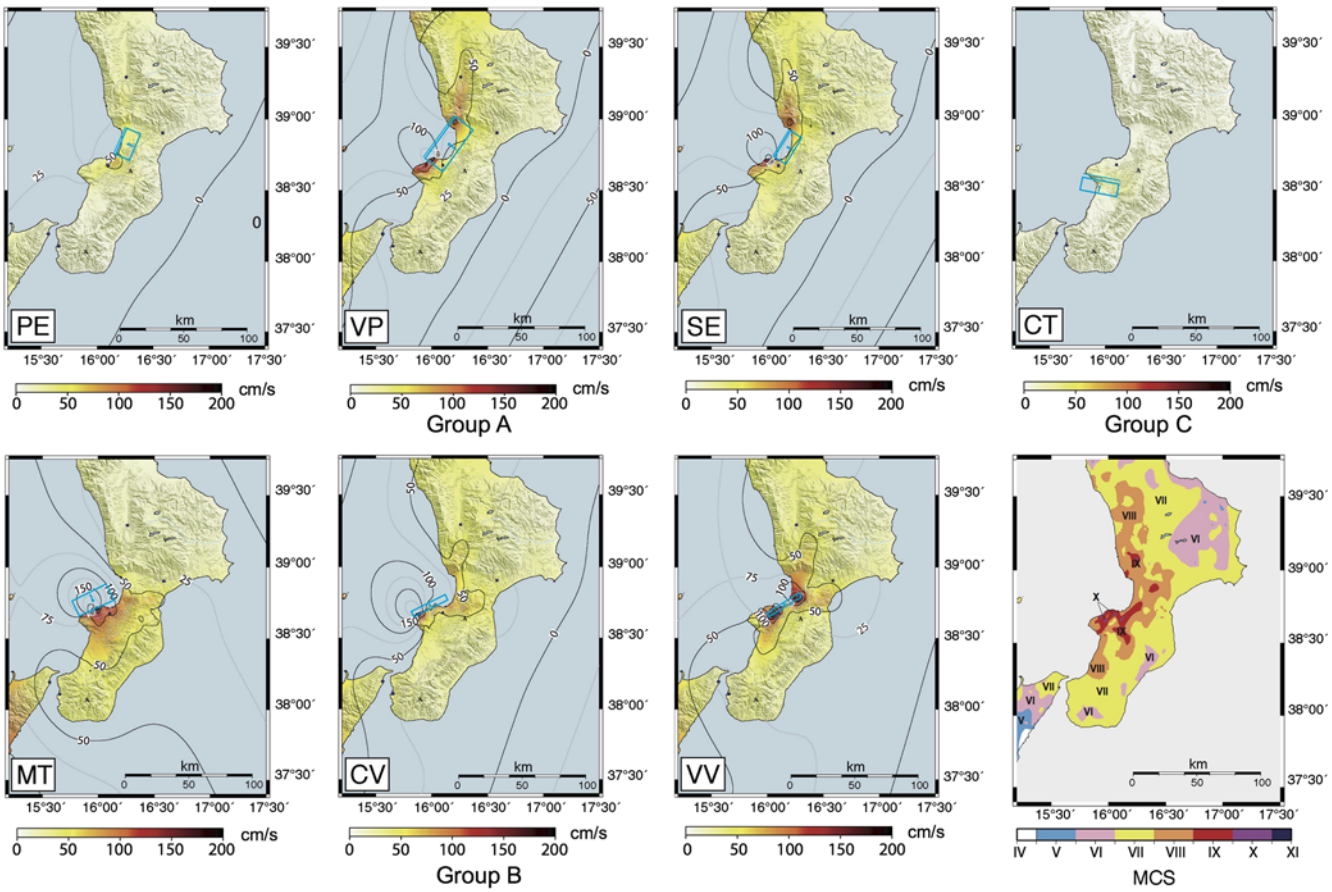

Figure 6. Maps of peak ground velocity (PGV) values calculated assuming bilateral rupture and uniform seismic moment distribution (U-case). Parameters for each source model are reported in Table 1. (Lower right) Intensities contour map. The color version of this figure is available only in the electronic edition.

low horizontal acceleration values, located far away from the area of maximum damage.

Figure 7 shows the PGV distribution for the seven models, assuming an M_0 distribution concentrated in a single asperity. Models in Group A exhibit a predominantly high PGV distribution, comparable with the I distribution. Except for the PE model, SE and VP models show two maxima in Pizzo (221 cm/s) and Curinga (143 cm/s). Models in Group B show generally low PGV values. Model VV includes two relative maxima, close to the cities of Vibo Valentia and Filadelfia. Model MT shows two relative high PGV values near Vibo Valentia and Tropea; these are higher than that shown by model VV. Group C (model CT) shows a trend similar to that of the uniform distribution case.

Assuming an M_0 distribution concentrated in two asperities (2A-case), the PGV radiation profiles show a general increase of maximum values (Fig. 8) if compared with the previous U- and 1A-cases (Figs. 6, 7). Models in Group A show a north-northeast-trending PGV distribution and maximum PGV values north of the Sant'Eufemia Gulf, near Lamezia Terme and Martinaro (X MCS; Fig. 4). Models SE and VP show a further relative maximum near Vibo Valentia. Group B shows a general PGV increase, centered on the Capo Vaticano promontory. Model VV records the maximum value at Triparni (320 cm/s versus X MCS; Figs. 4, 8). Model CV shows an absolute maximum at Tropea (360 cm/s), like model MT, although at lower PGV values. Finally, model CT (group C) shows very low PGV values well away from the 1905 mesoseismal area (Fig. 8).

To numerically test our ground-motion models, we converted calculated PGV values into I values and then compared them with MCS values. For all three cases (uniform, one asperity, and two asperity), we performed a conversion using the empirical regression by Faccioli and Cauzzi (2006). Moreover, we quantitatively assessed the robustness of the fit between calculated and observed I values as the sum of the quadratic residuals (Table 3). From a numerical perspective, we obtained the best results with model SE for the U-case (287 in Table 3) and with model VP for 1A-case (280 in Table 3). Conversely, SE and VP models returned the worst results for the 2A-case. For this case, we obtained the best result with model VV (349 in Table 3). Model CT produces residuals higher than all the models we analyzed (Table 3); however, we want to stress that these values are indicative of the overall reliability of the simulation in relation to the available intensity data.

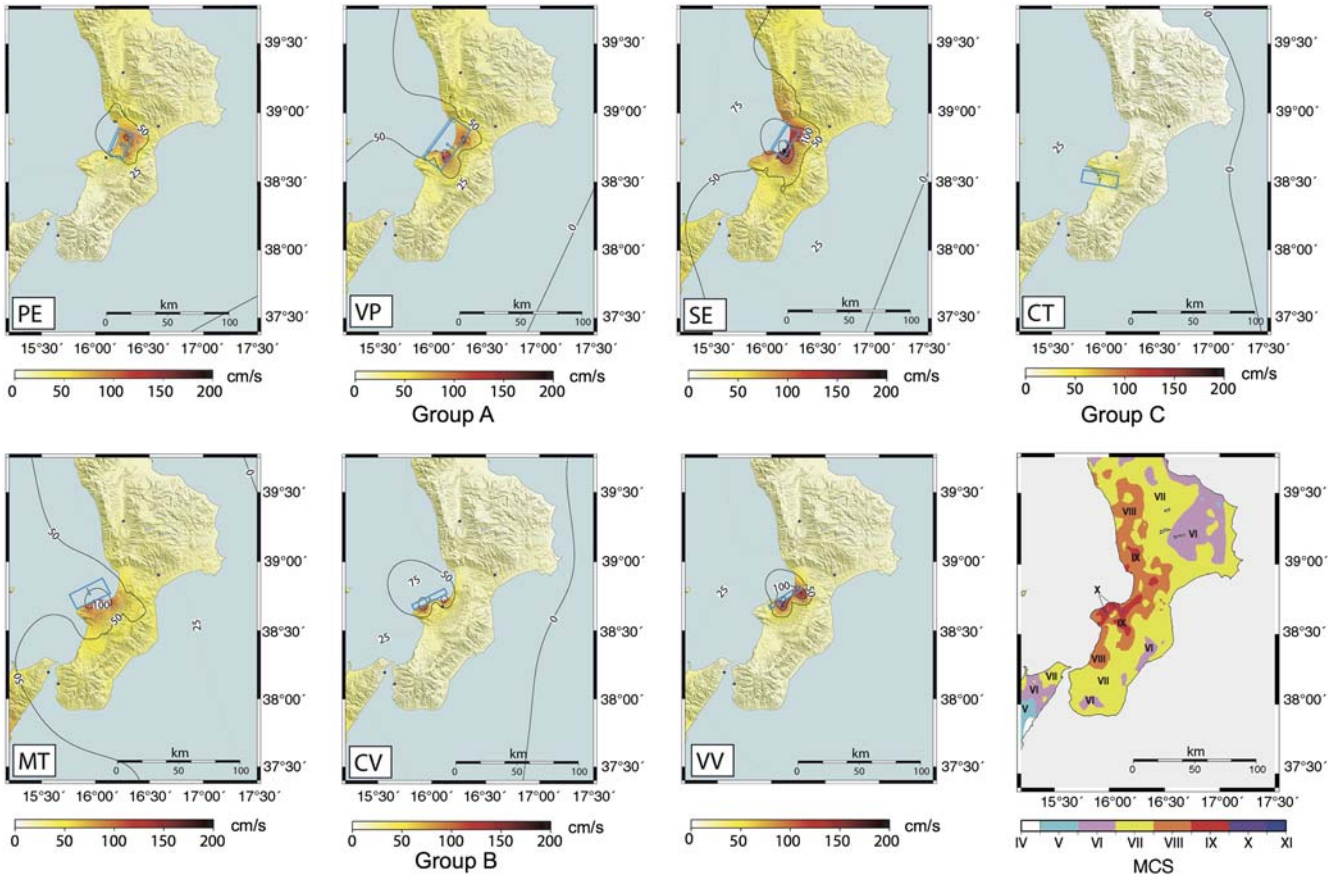

Figure 7. Maps of PGV values calculated assuming bilateral rupture and single asperity seismic moment distribution (1A-case). Parameters for each source model are reported in Table 1. (Lower right) Intensities contour map. The color version of this figure is available only in the electronic edition.

To verify the validity of the conversion method we used, we sorted the 421 observed macroseismic intensities values in descending order. The values of the observed intensities (small gray diamond in Fig. 9) are clustered in intensity classes of half a degree, and a square symbol indicates the median value of the population of each single bin. We then plotted the mean value of the calculated intensities for all the points belonging to the same class of the observed intensities (symbols in Fig. 9). In fact, a given class of observed intensities includes geographically scattered points, and each scenario produces different values, depending on the input model. The validity range for the empirical relationship proposed by Faccioli and Cauzzi (2006) lies between V and IX degrees (MCS); we thus dropped converted values outside of this range (denoted by a cross marked over the symbol in Fig. 9). For intensities $<$ VII, the derived values are always higher than the observed ones; conversely, for intensities $>$ VIII, observed values are always higher than the derived ones. Error increases toward the end members of intensities, that is, V and XI for observed and derived intensities, respectively.

Using the soil classification after Di Capua, Lanzo, *et al.* (2011) and Di Capua, Peppoloni, *et al.* (2011) (Table 2; Fig. 5), we also targeted possible site effects on observed intensities. Considering an amplification effect can be arguably expected for soft soil (types C and D), site conditions and short epicentral distances, we focused on sites with $I >$ IX, analyzing the behavior of the residuals (observed intensity minus calculated intensity) within 1° and at less than 20 km from the epicenter by Locati *et al.* (2011). Notice that a residual $(R) = 0$ indicates that the gap is within half a degree and is thus not considered meaningful. Figure 10 summarizes the residuals by soil type and epicentral distance. Because local amplification should be characterized by positive high residuals, for the SE 1A-case model, we identified sites on soil type C, such as Fitili, Parghelia, San Giovanni, and Zungri. Sites with $I =$ X (except Zammarù, with $I =$ XI) show residuals of 2. For soil type D, there are no cases (Fig. 10), whereas sites on soil type B are Limpidi, Mantineo, Paravati, Piscopio, and Triparni, mostly in the northern part of the Capo Vaticano promontory. Very similar results are also obtained for the VV model; on the other hand, the case with two asperities produces no evident effects on the distribution of the residuals.

Also, a few sites on the northern coast of the Capo Vaticano promontory that exhibit site effects, such as Zungri and Parghelia (on soil type C) and Triparni (on soil type B), are

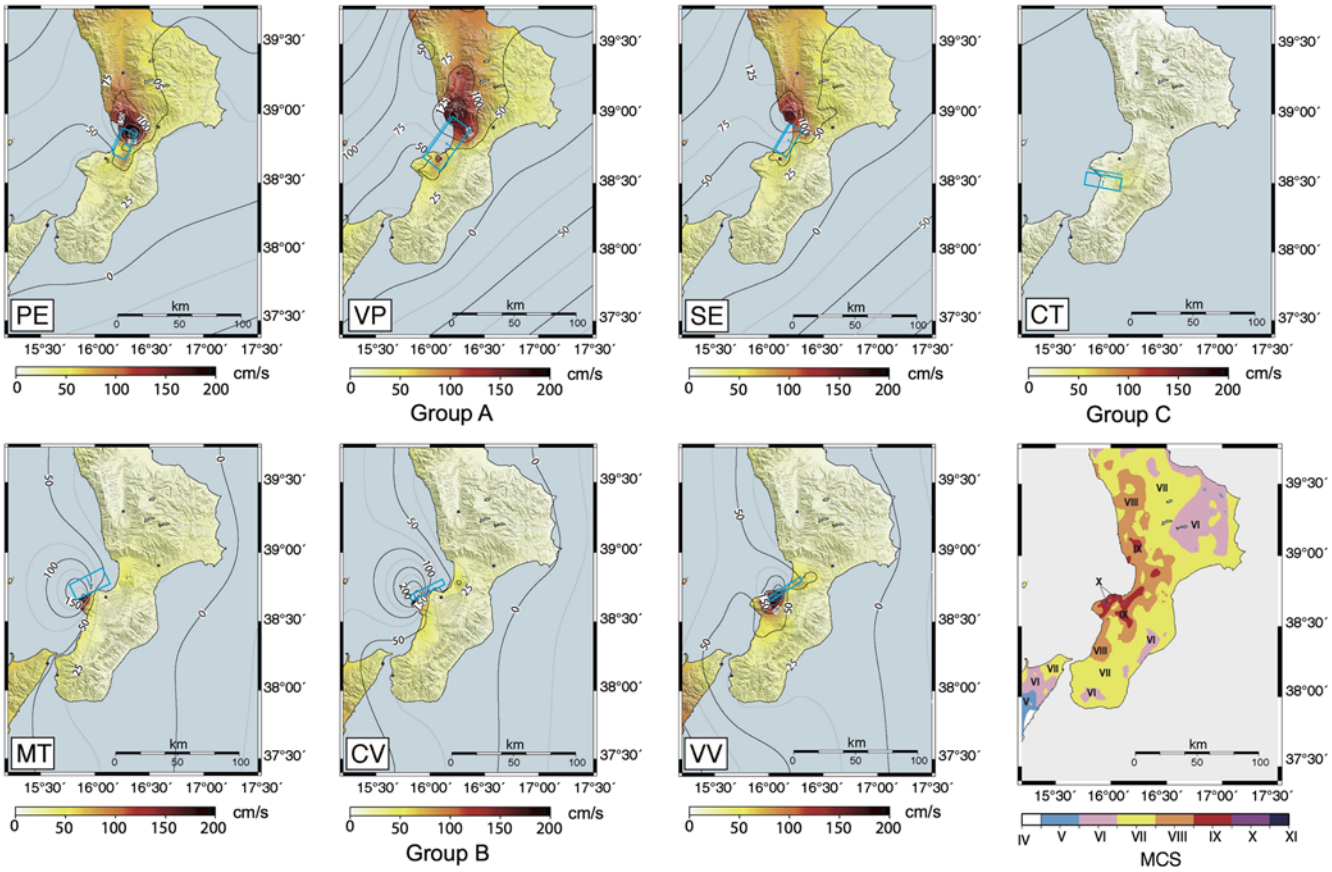

Figure 8. Maps of PGV values calculated assuming bilateral rupture and double asperity seismic moment distribution (2A-case). Parameters for each source model are reported in Table 1. (Lower right) Intensities contour map. The color version of this figure is available only in the electronic edition.

located over or close to reported landslides, some apparently triggered by or known at the time of the 8 September 1905 earthquake (see Progetto IFFI, 2006; Chiodo and Sorriso-Valvo, 2007; Porfido *et al.*, 2011; Progetto AVI, 2014).

Another aspect that deserves due consideration concerns the magnitude of this historical earthquake. In our modeling approach, once the normalized distribution of M_0 on the fault surface is chosen (Fig. 3), the magnitude is no more than a multiplicative factor. Assuming a magnitude uncertainty of ± 0.4, the seismic moment increases by a factor of 2.5. In turn, this translates into PGV values four times greater (or lesser) with respect to the mean value. For example, in the southeast 1A-case at the Briatico site (I = IX–X, Fig. 4), we obtain PGV = 140 cm/s (converted into I = IX) for M_w 6.8 (i.e., within the macroseismic estimates), whereas we get PGV = 557 cm/s (converted into I = X) from M_w 7.2 (closer to the instrumental estimates). In other words, a higher magnitude yielded much smaller residuals in the near field, within half a degree ($R = 0$) except for Zammarù (I = XI observed and I = IX calculated; Fig. 5c). The sites with $I <$ IX show negative residuals (i.e., the values obtained from modeling are higher), and globally the total sum of the quadratic residuals worsens—from 374 (Table 3) to 1325. Considering an M_w of 6.4, this value varies little compared with that obtained with M_w 6.8 (401). The result is a systematic increase of 1° in the near-field (20 km) residuals; residuals remain positive for $I >$ VII–VIII and taper to 0 for $I <$ VII. Small M_w fluctuations are evenly reflected in the energy distribution on the source in both the near and far field.

Table 3
Fit Values Obtained by All Models in Terms of the Residuals Quadratic Sum, Broken Down in the Three Groups (A, B, and C)

ID	Group	U Case	1A Case	2A Case
PE	A	296	326	526
VP		300	280	502
SE		287	374	420
MT	B	404	404	402
CV		337	295	362
VV		394	315	349
CT	C	875	554	873

U, 1A, and 2A cases indicate the choice of the seismic moment distribution on the source plane.

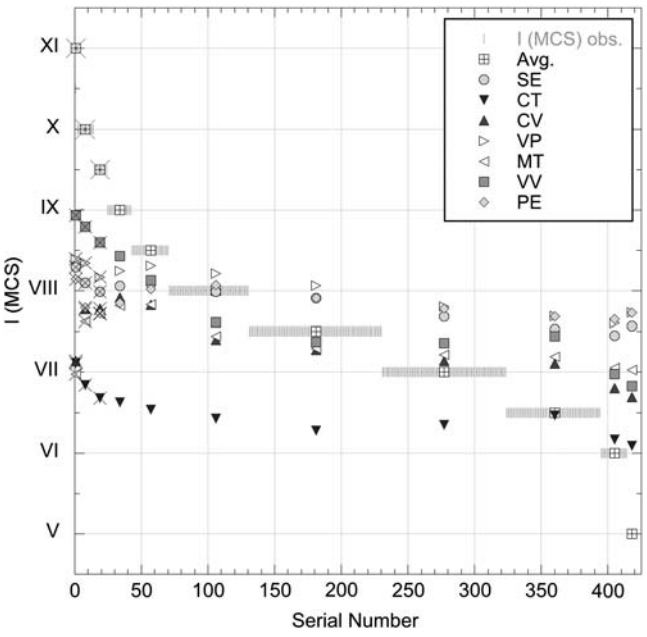

Figure 9. Observed macroseismic intensities (small vertical bars), sorted in descending order, with the median value of each single bin (large square). We also plot the mean value of the calculated intensities for datapoints belonging to the same class of the observed intensity (symbols). A cross marked over a symbols cuts away the values outside the validity range for the conversion relationship (V–IX).

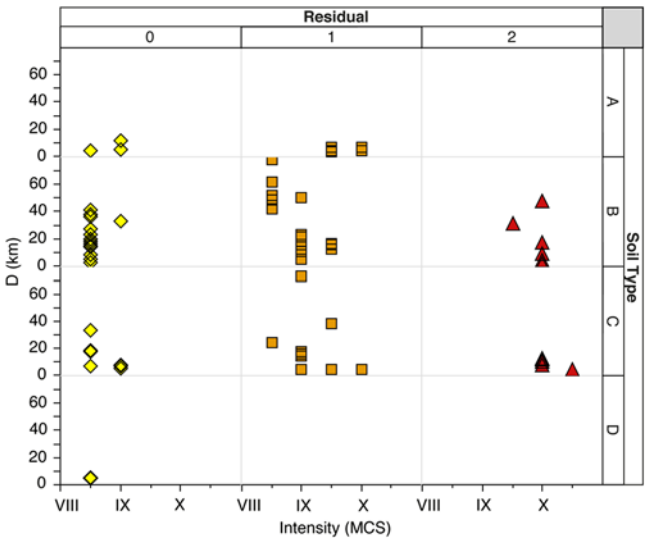

Figure 10. Intensity sites with I > IX. Distribution of the residuals (observed intensity—calculated intensity) grouped into classes of intensity equal to 1°, as a function of epicentral distance (see D on the left) and soil type at the given site. The color version of this figure is available only in the electronic edition.

Discussions and Conclusions

Model Results and Shaking Scenarios

The intent of this article is to contribute to better constrain the seismogenic source of the 8 September 1905 Calabria earthquake. To achieve this goal, we calculated ground-motion scenarios for the fault models documented in the literature (see Table 1) as the causative source of this destructive yet poorly understood event. To double check our results, we numerically compared them with the recorded intensity distribution.

Modeling ground-shaking scenarios is affected by intrinsic restrictions. These include the following: (1) uncertainties in the definition of input fault models and their location, (2) limits of the method to compute synthetic seismograms, (3) uncertainties and limits of applicability of the empirical relationships to convert PGV into equivalent MCS values, and (4) uncertainties affecting maximum intensities estimates (i.e., when the macroseismic field of a damaging earthquake includes complexities due to location, terrain, age, and suspected site effects).

We analyze the shaking scenarios by the respective source model and group, starting from the one that includes only one model. Group C consists of the CT model (Coccorino fault; Table 1) proposed by Cucci and Tertulliani (2006, 2010; see also Tertulliani and Cucci, 2008, 2009), which was the worst performing of all the models (U-, 1A-, and 2A-cases in Figs. 6–8, respectively). Such an outcome is also confirmed by the very high residuals obtained with the intensity conversion (Table 3). Based on these results and considering its location well away from the 1905 mesoseismal area, we doubt the CT model may be considered as a possible source for the 1905 earthquake.

Of the Group A models, the PE model proposed by Peruzza *et al.* (1997) was the least compatible with the MCS distribution, especially in U- and 1A-cases (Figs. 6, 7), although the fit improves in the 2A-case (Fig. 8). This model also results in high residuals, which worsen with fault-plane complexity (Table 3). The results of ground-shaking modeling and the lack of evidence of fault activity close to the shoreline, at least based on the available data, lead us to believe that the PE model cannot be considered as the causative source of the 1905 event. On the other hand, the VP model (also Group A) proposed by Valensise and Pantosti (2001) yields a fairly good fit between PGV and MCS values (Figs. 6–8). For the 1A-case, VP shows the best results in terms of residuals quadratic values (280; Table 3). In spite of this, no evidence of such fault was recognized on geophysical data acquired within the Sant'Eufemia Gulf by Loreto *et al.* (2012); such data led Loreto *et al.* (2013) to identify a normal fault (SE model), closer to the shoreline, with similar dip and strike (Table 1) to the VP model.

The SE model (Group A) proposed by Loreto *et al.* (2013) yields a good fit between high PGV and MCS values for the U- and 2A-cases (Figs. 6, 8) and a very good fit for the 1A-case (Fig. 7). Such results, however, are not confirmed by residuals, which were higher for the 1A-case (374; Table 3) and the lowest for the U-case (e.g., 287; Table. 3). This seeming contradiction could be due to the conversion law used to derive intensities from PGV values (Fig. 9), which tends to

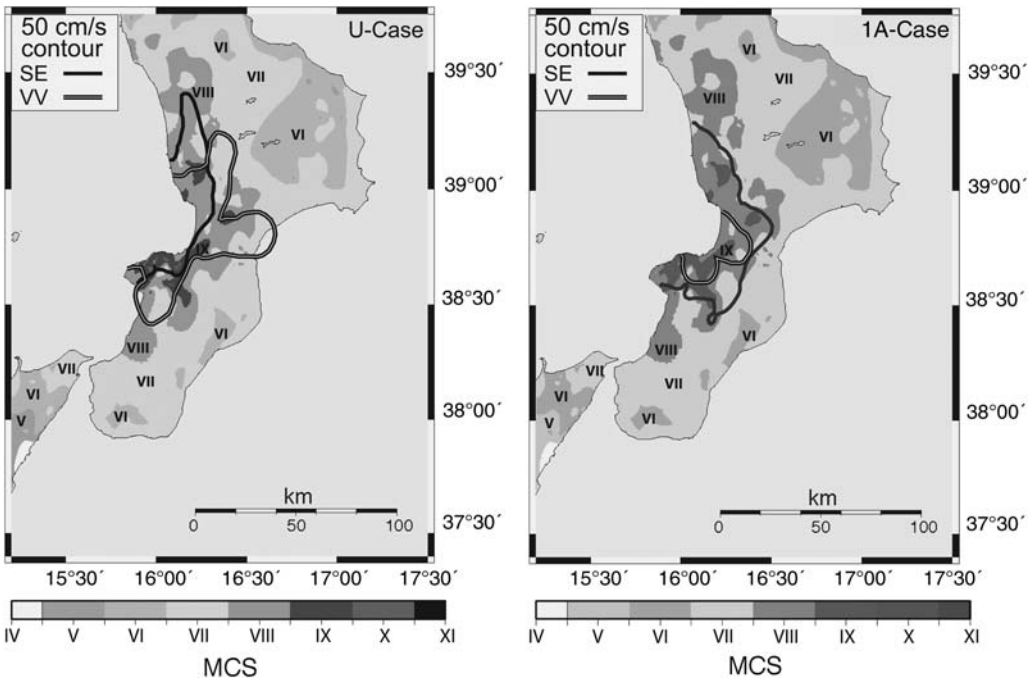

Figure 11. PGV contour line at 50 cm/s including most of the mesoseismal area from the SE and VV models versus intensity pattern for U- and 1A-cases.

favor intermediate values over high and/or low end members (see also the above paragraph). Despite this mismatch, the very good shaking-scenario results, combined with the convincing tectonic features associated with this model (Loreto *et al.*, 2013), allow us to identify the SE model as the best candidate, among models in Group A, as the causative source of the 1905 earthquake.

Ground-shaking scenarios for Group B models MT (proposed by Monaco and Tortorici, 2000) and CV (parameterized by Piatanesi and Tinti, 2002) are characterized by a decreasing fit between PGV and MCS values with increasing fault-plane complexity (Figs. 6–8). Moreover, the MT model provides fairly high residual values for all analyzed cases (> 400; Table 3). The CV model provides a low residual for the 1A-case (295; Table 3) and fairly good tsunami simulation results (Piatanesi and Tinti, 2002). Nevertheless, the southward-trending radiation velocity profile suggests the CV model is not adequately located with respect to the damage distribution, especially for the 1A- and 2A-cases. Accordingly, we deem both the CV and MT sources the least suitable, among models in Group B, as the causative source of the 1905 earthquake.

Finally, the VV model (Group B), proposed by Piatanesi and Tinti (2002) and based on interpretations by Monaco and Tortorici (2000), shows the best high PGV distribution compared with MCS data for the U-case (Fig. 6), although the fit worsens with increasing fault-plane complexity (1A- and 2A-cases; Figs. 7, 8). In spite of this, the good fit for the U-case is not supported by the very high residuals (394; Table 3), but it improves in the 1A-case (315; Table 3). As for the SE model, we believe this contradiction is due to the conversion law used. Accordingly, among models in Group B, we take the VV model into account as a potential source of the 1905 earthquake.

Models Versus MCS Distribution

Considering the residual values are larger with increasing fault-plane complexity for all seven source models (Table 3), we can reasonably rule out the possibility of a source plane being affected by two or more asperities. The above synthesis of our results (see the Model Results and Shaking Scenarios section) allows us to identify two models, SE and VV, as the most probable causative sources—although for different dynamic conditions. The SE model provides the best fit for the 1A-case; whereas the VV model yields the best fit for the U-case. To look further into this interesting and somewhat puzzling result, we plotted the PGV 50 cm/s contour line, taken from the shaking scenarios of the SE and VV models for both the U- and the 1A-cases, over the MCS distribution (Fig. 11). We chose the 50 cm/s value, because it corresponds to nearly the VI–VII MCS degrees. As noted earlier, these are the values that best satisfy the conversion law (Fig. 9), and this contour line includes the damaging sector of the 1905 mesoseismal area (MCS > VIII).

Assuming a source plane with one asperity (1A-case), the SE model provides the best fit with the area of maximum damage. Despite the high residuals (374; Table 3), the comparison between the converted and the observed intensities allows us to favor the SE model over the VV one (Fig. 12). Considering both U- and 1A-cases, intensities converted from the SE model provide the best fit for class VIII

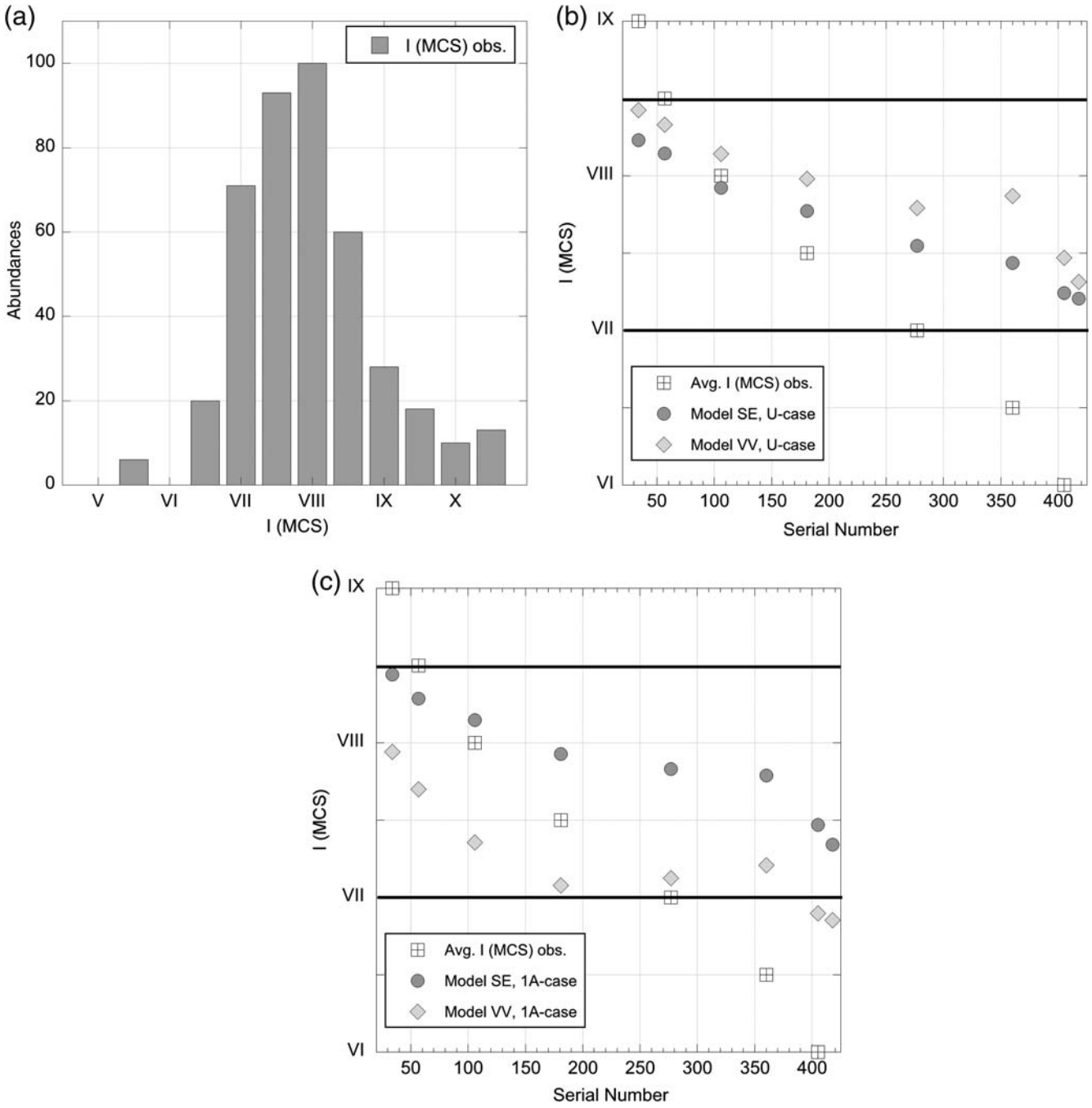

Figure 12. (a) Distribution of the MCS intensity dataset (421 total amount) used in our comparative analysis. (b) Average value of macroseismic intensities, sorted in descending order, plotted in correspondence to the central value of each class bin. Gray squares show observed intensities, and circles indicate converted intensities for the SE and VV models in the U-case. (c) Same as in (b) but in the 1A-case.

(MCS; Figs. 12b,c), which, together with class VII–VIII, correspond to the most abundant recorded intensities (Fig. 12a). Moreover, for higher intensity classes (> VIII MCS), the SE model shows the best fit for the 1A-case and a fairly good fit for the U-case. Such fit strongly worsens for lower classes in the 1A-case (Fig. 12c), in which case the VV model is favored. Accordingly, we reasonably take the SE model as the one that seems to most adequately fit the observed intensity distribution, particularly for the mesoseismal area.

Site Effects and Source Complexities?

There is at least one additional factor that may help to explore some complexities and seeming contradictions. As noted in earlier paragraphs, some of the higher observed-intensity data points lie on the northern slope of the Capo Vaticano promontory. This area, like several others throughout the Calabrian landmass, is reportedly affected by extensive landslide phenomena (for overviews, see Progetto IFFI,

2006, and Progetto AVI, 2014). Some of these features may also have been triggered by the 8 September 1905 event (Chiodo and Sorriso-Valvo, 2007; Porfido *et al.*, 2011) or by one of the major seismic crises that previously devastated western Calabria (Porfido *et al.*, 2011). Without *ad hoc* data (i.e., horizontal-to-vertical spectral ratio; e.g., Nakamura, 1989) that go beyond the scope of this article, it is clearly difficult to establish a direct, univocal link between those sites in this area with $I \geq$ IX and an amplification effect due to either inherited slope instabilities or other landslide-related features. However, we notice that such sites concentrate on soil types B and C (Fig. 10) in the near field, that is, on gradually softer (less cohesive?) deposits. If this circumstance may have influenced (i.e., raised) the observed intensities in the core of the maximum damage area, it may also have led to potentially higher (less reliable?) macroseismic M_w estimates (see the earthquake sizing procedures in Gasperini *et al.*, 1999, 2010).

Based on the above lines of reasoning and on the available data, we maintain that, among the seven literature models, two appear to be the most suitable as the potential source of the 1905 earthquake: the Sant'Eufemia fault (SE) and the Vibo Valentia fault (VV). These two models, however, best fit either observed MCS data and/or synthetic PGV patterns, depending on different dynamic conditions, which makes the two possible solutions not easy to reconcile or to choose among—unless one goes back to the geological pattern of western Calabria, where it all started on 8 September 1905. In fact, although only the SE fault was recognized on geophysical data, the two faults are sub-parallel, dip toward each other, and form what could be regarded as a graben. Similar tectonic relations are common in the back-arc system along the western Calabrian arc (Doglioni *et al.*, 1999), including the source of the well-known catastrophic 1908 Messina-Reggio Calabria earthquake (M_w 7.1) (Bonini *et al.*, 2011).

Therefore, we believe that although the SE model seems to fit the damage pattern better than the VV one does, the dual solution that we draw could derive from either (1) further source complexities within SE (dynamic and/or geometric) and/or (2) fault interaction in the tectonic pattern of the Sant'Eufemia Gulf. Further studies could reveal where those heterogeneities may lie, from either a fault dynamics or kinematic viewpoint.

Data and Resources

All data used in this article came from the published sources listed in the references. Some plots were made using Generic Mapping Tools v.4.5.7 (http://www.soest.hawaii.edu/gmt; Wessel and Smith, 1998). The following online databases were used: Progetto IFFI, Inventario dei Fenomeni Franosi in Italia (http://www.sinanet.isprambiente.it/progettoiffi); Progetto AVI, Archivio frane—Sistema Informativo sulle Catastrofi Idrogeologiche, Istituto di Ricerca per la Protezione Idrogeologica, Consiglio Nazionale delle Ricerche (http://sici.irpi.cnr.it/avi.htm); CFTI4Med, Catalogue of Strong Earthquakes in Italy (461 B.C.–1997) and Mediterranean area (760 B.C.–1500) (http://storing.ingv.it/cfti4med/; Guidoboni *et al.*, 2007); Catalogo Parametrico dei Terremoti Italiani, Versione 2004 (CPTI04) (http://emidius.mi.ingv.it/CPTI04/; Gruppo di Lavoro CPTI, 2004); CPTI11, the 2011 version of the Parametric Catalogue of Italian Earthquakes (http://emidius.mi.ingv.it/CPTI/; Rovida *et al.*, 2011); DBMI11, the 2011 version of the Italian Macroseismic Database (http://emidius.mi.ingv.it/DBMI11; Locati *et al.*, 2011); Italian Seismological Instrumental and Parametric Database (http://iside.rm.ingv.it; ISIDe Working Group, 2010); Database of Individual Seismogenic Sources (http://diss.rm.ingv.it/diss/; DISS Working Group, 2010); and Global Historical Tsunami Database (http://www.ngdc.noaa.gov/hazard/tsu_db.shtml; NGDC/WDC, 2012). Gomez Capera *et al.* (2007) is available at http://esse1.mi.ingv.it/d7.html. All URLs were last accessed in August 2014.

Acknowledgments

This work was developed within the project ISTEGE, "Indagine Sismotettonica del TErremoto dell'8 Settembre 1905 (M_w 7.4) nel Golfo di Sant'Eufemia—offshore tirrenico calabrese," supported by the Istituto Nazionale di Oceanografia e di Geofisica Sperimentale (OGS). This article greatly benefited from the constructive points raised by the two reviewers and Associate Editor M. Stirling. Also, we thank P. Vannoli, P. Burrato, and G. Valensise (Istituto Nazionale di Geofisica e Vulcanologia) for fruitful scientific discussions. This is Istituto di Scienze Marine-Consiglio Nazionale delle Ricerche (ISMAR-CNR) Contribution Number 1852 (Ritmare Project).

References

Atkinson, G. M. (2001). Linking historical intensity observations with ground-motion relations for eastern North America, *Seismol. Res. Lett.* **72,** 560–574.

Bakun, W. H., and C. M. Wentworth (1997). Estimating earthquake location and magnitude from seismic intensity data, *Bull. Seismol. Soc. Am.* **87,** no. 6, 1502–1521.

Baratta, M. (1906). Il grande terremoto calabro dell'8 settembre 1905, *Atti Soc. Tosc. Sc. Nat.* **22,** 57–80 (in Italian).

Barone, M., R. Dominici, F. Muto, and S. Critelli (2008). Detrital modes in a Late Miocene wedge-top basin, northeastern Calabria, Italy: Compositional record of wedge-top partitioning, *J. Sediment. Res.* **78,** 693–711.

Basili, R., G. Valensise, P. Vannoli, P. Burrato, U. Fracassi, S. Mariano, M. M. Tiberti, and E. Boschi (2008). The Database of Individual Seismogenic Sources (DISS), version 3: Summarizing 20 years of research on Italy's earthquake geology, *Tectonophysics* **453,** 20–43, doi: 10.1016/j.tecto.2007.04.014.

Boatwright, J., K. Thywissen, and L. C. Seekins (2001). Correlation of ground motion and intensity for the 17 January 1994 Northridge, California, earthquake, *Bull. Seismol. Soc. Am.* **91,** no. 4, 739–752.

Bommer, J., and J. E. Alarcon (2006). The prediction and use of peak ground velocity, *J. Earthq. Eng.* **10,** 1–31.

Bonardi, G., W. Cavazza, V. Perrone, and S. Rossi (2001). Calabria-28 Peloritani terrane and northern Ionian Sea, in I. P. Martini and G. B. Vai (Editors), *Anatomy of an Orogen: The Apennines and Adjacent Mediterranean Basins*, Kluwer Academic Publishers, Dordrecht, The Netherlands, 287–306.

Bonini, L., D. Di Bucci, G. Toscani, S. Seno, and G. Valensise (2011). Reconciling deep seismogenic and shallow active faults through analogue modelling: The case of the Messina Straits (southern Italy), *J. Geol. Soc. London* **168,** 191–199, doi: 10.1144/0016-76492010-055.

Bordoni, P., and G. Valensise (1998). Deformation of the 125 ka marine 29 terrace in Italy: Tectonic implications, in *Late Quaternary Coastal Tectonics*, I. Stewart and C. Vita Finzi (Editors), Geol. Soc. London Spec. Publ. 146, 71–110, doi: 10.1144/GSL.SP.1999.146.01.05.

Boschi, E., E. Guidoboni, G. Ferrari, D. Mariotti, G. Valensise, and P. Gasperini (2000). Catalogue of strong Italian earthquakes from 461 B.C. to 1997, *Ann. Geofisc.* **43,** 259.

Camassi, R., and M. Stucchi (1997). *NT4.1.1, un catalogo parametrico di terremoti di area italiana al di sopra della soglia del danno*, Gruppo Naz. Difesa Terremoti, Milan, Italy, 95 pp. (in Italian).

Cara, F., A. Rovelli, G. Di Giulio, F. Marra, T. Braun, G. Cultrera, R. Azzera, and E. Boschi (2005). The role of site effects on the intensity anomaly of San Giuliano di Puglia inferred from aftershocks of the Molise, central southern Italy, sequence, November 2002, *Bull. Seismol. Soc. Am.* **95,** no. 4, 1457–1468, doi: 10.1785/0120040031.

Castro, R. R., F. Pacor, A. Sala, and C. Petrungaro (1996). *S* wave attenuation and site effects in the region of Friuli, Italy, *J. Geophys. Res.* **101,** no. B10, 2156–2202, doi: 10.1029/96JB02295.

Catalano, S., G. De Guidi, C. Monaco, G. Tortorici, and L. Tortorici (2003). Long-term behavior of the late Quaternary normal faults in the Straits of Messina area (Calabrian arc): Structural and morphological constraints, *Quaternary Int.* **101/102,** 81–91, doi: 10.1016/S1040-6182(02)00091-5.

Chiodo, G., and M. Sorriso-Valvo (2007). Frane sismo-indotte: Casistica e fenomeni innescati dal terremoto dell'8 settembre 1905, in *Aspetti dei rischi naturali in Calabria*, I. Guerra (Editor), Università della Calabria, AGM, Castrovillari, Italy, 57–71 (in Italian).

Costa, G., G. F. Panza, P. Suhadolc, and F. Vaccari (1993). Zoning of the Italian territory in terms of expected peak ground acceleration derived from complete synthetic seismograms, *J. Appl. Geophys.* **30,** 1–12.

Cucci, L., and A. Tertulliani (2006). I terrazzi marini nell'area di Capo Vaticano (arco calabro): Solo un record di sollevamento regionale o anche di deformazione cosismica? *Il Quaternario (Italian J. Quatern. Sci.)* **19,** 89–101 (in Italian).

Cucci, L., and A. Tertulliani (2010). The Capo Vaticano (Calabria) coastal terraces and the 1905 **M** 7 earthquake: The geomorphological segnature of the regional uplift and coseismic slip in southern Italy, *Terra Nova* **22,** no. 5, 378–389, doi: 10.1111/j.1365-3121.2010.00961.x.

Das, S., and P. Suhadolc (1996). On the inverse problem for earthquake rupture: The Haskell-type source model, *J. Geophys. Res.* **101,** 5725–5738.

Database of Individual Seismogenic Sources (DISS) Working Group (2010). *Database of Individual Seismogenic Sources (DISS), Version 3.1.1: A Compilation of Potential Sources for Earthquakes Larger than M 5.5 in Italy and Surrounding Areas*, INGV 2010—Istituto Nazionale di Geofisica e Vulcanologia, doi: 10.6092/INGV.IT-DISS3.1.1.

Del Ben, A., C. Barnaba, and A. Taboga (2008). Strike-slip systems as the main tectonic features in the Plio-Quaternary kinematics of the Calabrian arc, *Mar. Geophys. Res.* **29,** 1–12, doi: 10.1007/s11001-007-9041-6.

Dewey, J. F., M. L. Helman, E. Turco, D. H. W. Hutton, and S. D. Knott (1989). Kinematics of the western Mediterranean, in *Alpine Tectonics*, M. P. Coward, D. Dietrich, and R. G. Park (Editors), Geol. Soc. London Spec. Publ. 45, 265–283, doi: 10.1144/GSL.SP.1989.045.01.15.

Di Capua, G., G. Lanzo, V. Pessina, S. Peppoloni, and G. Scasserra (2011a). The recording stations of the Italian strong motion network: Geological information and site classification, *Bull. Earthq. Eng.* **9,** 1779–1796, doi: 10.1007/s10518-011-9326-7.

Di Capua, G., S. Peppoloni, M. Amanti, C. Cipolloni, G. Conte, D. Avola, A. Del Buono, E. Borgomeo, C. Negri Arnoldi, and S. Scrivieri (2011b). Il Progetto SEE-GeoForm: Uno strumento per la consultazione di dati geologici e di pericolosità sismica riferiti all'intero territorio nazionale, *ANIDIS 2011—XIV National Congress "L'ingegneria sismica in Italia"*, Bari, Italy, 18–22 September 2011 (in Italian).

Doglioni, C., P. Harabaglia, S. Merlini, F. Mongelli, A. Peccerillo, and C. Piromallo (1999). Orogens and slabs vs their direction of subduction, *Earth Sci. Rev.* **45,** 167–208, doi: 10.1016/S0012-8252(98)00045-2.

Faccenna, C., T. W. Becker, F. P. Lucente, L. Jolivet, and F. Rossetti (2001). History of subduction and back-arc extension in the central Mediterranean, *Geophys. J. Int.* **145,** 809–820, doi: 10.1046/j.0956-540x.2001.01435.x.

Faccenna, C., T. W. Becker, M. S. Miller, E. Serpelloni, and S. D. Willett (2014). Isostasy, dynamic topography, and the elevation of the Apennines of Italy, *Earth Planet. Sci. Lett.* **407,** 163–174, doi: 10.1016/j.epsl.2014.09.027.

Faccioli, E., and C. Cauzzi (2006). Macroseismic intensities for seismic scenarios, estimated from instrumentally based correlation, in *Conf. Proc., First European Conference on Earthquake Engineering and Seismology*, Geneva, Switzerland, 3–8 September 2006, Paper Number 569, 1–10.

Faenza, L., and A. Michelini (2010). Regression analysis of MCS intensity and ground motion parameters in Italy and its application in ShakeMap, *Geophys. J. Int.* **180,** 1138–1152, doi: 10.1111/j.1365-246X.2009.04467.x.

Fitzko, F., P. Suhadolc, and G. Costa (2004). Realistic strong ground motion scenarios for seismic hazard assessment studies at the Alp-Dinarides Junction, in *Earthquake: Hazard, Risk, and Strong Ground Motion*, Y. T. Chen, G. F. Panza, and Z. L. Wu (Editors), Seismological Press, Beijing, China, 361–377.

Florsch, N., D. Fah, P. Suhadolc, and G. F. Panza (1991). Complete synthetics seismograms for high frequency multimode *SH* waves, *Pure Appl. Geophys.* **136,** 529–560.

Fracassi, U., D. Di Bucci, D. Ridente, F. Trincardi, and G. Valensise (2012). Recasting historical earthquakes in coastal areas (Gargano Promontory, Italy): Insights from marine paleoseismology, *Bull. Seismol. Soc. Am.* **102,** no. 1, 1–17, doi: 10.1785/0120110001.

Gallipoli, M. R. (1999). Monitoraggio sismico con stazioni digitali ad alta 32 risoluzione: Primi risultati, Istituto di Metodologie per l'Analisi Ambientale, Consiglio Nazionale delle Ricerche (IMAA-CNR), *Technical Report 7/99* (in Italian).

Gasperini, P., F. Bernardini, G. Valensise, and E. Boschi (1999). Defining seismogenic sources from historical earthquake felt reports, *Bull. Seismol. Soc. Am.* **89,** no. 1, 94–110.

Gasperini, P., G. Vannucci, D. Tripone, and E. Boschi (2010). The location and sizing of historical earthquakes using the attenuation of macroseismic intensity with distance, *Bull. Seismol. Soc. Am.* **100,** no. 5A, 2035–2066, doi: 10.1785/0120090330.

Ghisetti, F. (1984). Recent deformations and the seismogenic source in the Messina Strait (southern Italy), *Tectonophysics* **109,** 191–208.

Gomez Capera, A. A., C. Meletti, A. Rebez, and M. Stucchi (2007). Mappe di pericolosità sismica in termini di intensità macrosismica ottenute utilizzando lo stesso impianto metodologico di MPS04, *Progetto INGV-DPC S1*, Deliverable D7 (in Italian).

Gruppo di Lavoro CPTI (2004). *Catalogo Parametrico dei Terremoti Italiani, Versione 2004 (CPTI04)*, Istituto Nazionale di Geofisica e Vulcanologia (INGV), Bologna, Italy, doi: 10.6092/INGV.IT-CPTI04 (in Italian).

Guidoboni, E., and J. E. Ebel (2009). *Earthquakes and Tsunamis in the Past*, Cambridge University Press, Cambridge, United Kingdom, 590 pp.

Herrero, A., and P. Bernard (1994). A kinematic self-similar rupture process for earthquakes, *Bull. Seismol. Soc. Am.* **84,** 1216–1228.

ISIDe Working Group (2010). Italian seismological instrumental and parametric database, http://iside.rm.ingv.it (last accessed August 2014).

Kaka, S. I., and G. M. Atkinson (2004). Relationships between instrumental ground-motion parameters and modified Mercalli intensity in eastern North America, *Bull. Seismol. Soc. Am.* **94,** no. 5, 1728–1736.

Kanamori, H., and D. L. Anderson (1975). Theoretical basis of some empirical relations in seismology, *Bull. Seismol. Soc. Am.* **65,** no. 5, 1073–1095.

Knott, S. D., and E. Turco (1991). Late Cenozoic kinematics of the Calabrian arc, southern Italy, *Tectonics* **10,** no. 6, 1164–1172.

Locati, M., R. Camassi, and M. Stucchi (Editors) (2011). *DBMI11, la versione 2011 del Database Macrosismico Italiano*, Milano, Bologna, doi: 10.6092/INGV.IT-DBMI11.

Loreto, M. F., U. Fracassi, A. Franzo, P. Del Negro, F. Zgur, and L. Facchin (2013). Approaching the seismogenic source of the Calabria 8 September 1905 earthquake: New geophysical, geological and biochemical data from the S. Eufemia Gulf (S Italy), *Mar. Geol.* **343,** 62–75, doi: 10.1016/j.margeo.2013.06.016.

Loreto, M. F., F. Zgur, L. Facchin, U. Fracassi, F. Pettenati, I. Tomini, M. Burca, P. Diviacco, C. Sauli, and G. Cossarini, et al. (2012). In search of new imaging for historical earthquakes: A new geophysical survey offshore western Calabria (southern Tyrrhenian Sea, Italy), *Boll. Geofis. Teor. Appl.* **53,** no. 4, 385–401.

Malinverno, A., and W. B. F. Ryan (1986). Extension in the Tyrrhenian Sea and shortening in the Apennines as result of arc migration driven by sinking of the lithosphere, *Tectonics* **5,** 227–245.

Martini, M., and R. Scarpa (1982). Earthquakes in Italy in the last century. In earthquakes: observation, theory and interpretation, H. Kanamori and E. Boschi (Editors), in *Proc. Enrico Fermi Summer School in Geophysics*, Varenna, Italy, LXXXV course, 479–492.

Michelini, A., A. Lomax, A. Nardi, and A. Rossi (2006). La localizzazione del terremoto della Calabria dell'8 settembre 1905 da dati strumentali, in *8 Settembre 1905, Terremoto in Calabria*, I. Guerra and A. Bavaglio (Editors), Università della Calabria, 225–240 (in Italian)

Monaco, C., and L. Tortorici (2000). Active faulting in the Calabrian arc and eastern Sicily, *J. Geodyn.* **29,** 407–424.

Mucciarelli, M., G. Valensise, M. R. Gallipoli, and R. Caputo (2000). Reappraisal of a XVI century earthquake combining historical, geological and instrumental information, in V. Castelli (Editor), *Proceedings of Workshop of ESC Sub.-Comm. on Historical Seismology*, Macerata, Italy, 1999.

Mulargia, F., P. Balsi, V. Achilli, and F. Broccio (1984). Recent crustal deformations and tectonics of the Messina Strait area, *Geophys. J. Int.* **76,** 369–386.

Nakamura, Y. (1989). A method for dynamic characteristics estimation of subsurface using microtremor on the ground surface, *Q. Rep. Railway Tech. Res. Inst.* **30,** no. 1, 25–33.

National Geophysical Data Center/World Data Service (NGDC/WDS) (2012). *Global Historical Tsunami Database*, National Geophysical Data Center, NOAA, Boulder, Colorado, doi: 10.7289/V5PN93H7.

Norme Tecniche per le Costruzioni (NTC) (2008). Norme Tecniche per le Costruzioni, DM 14 gennaio 2008, *Gazzetta Ufficiale*, n. 29 del 4 February 2008, Supplemento Ordinario n. 30, Istituto Poligrafico e Zecca dello Stato, Roma, 654 pp. (in Italian).

Orecchio, B., D. Presti, C. Totano, and G. Neri (2014). What earthquakes say concerning residual subduction and STEP dynamics in the Calabrian arc region, south Italy, *Geophys. J. Int.* **199,** 1929–1942, doi: 10.1093/gji/ggu373.

Panza, G. F. (1985). Synthetics seismograms: The Rayleigh waves modal summation, *J. Geophys.* **58,** 125–145.

Panza, G. F., and P. Suhadolc (1987). Complete strong motion synthetics, in *Seismic Strong Motion Synthetics*, B. A. Bolt (Editor), Academic Press, Orlando, Florida, 153–204.

Panza, G. F., F. Romanelli, and F. Vaccari (2001). Seismic wave propagation in laterally heterogeneous anelastic media: Theory and applications to seismic zonation, *Adv. Geophys.* **43,** 1–95, doi: 10.1016/S0065-2687(01)80002-9.

Patacca, E., and P. Scandone (2004). The Plio-Pleistocene thrust belt—Foredeep system in the southern Apennines and Sicily (Italy), in *Geology of Italy*, U. Crescenti, S. D'Offizi, S. Merlini, and L. Lacchi (Editors), Soc. Geol. It., Roma, Italy, 93–129.

Patacca, F., R. Sartori, and P. Scandone (1990). Tyrrhenian basin and Apenninic arcs: Kinematic relations since Late Tortonian times, *Mem. Soc. Geol. It.* **45,** 425–451.

Patacca, F., R. Sartori, and P. Scandone (1993). Tyrrhenian basin and Apennines: Kinematic evolution and related dynamic constraints, in *Recent Evolution and Seismicity of the Mediterranean Region*, E. Boschi, E. Mantovani, and A. Morelli (Editors), Kluwer Academic Publisher, Dordrecht, Netherlands, 161–171.

Peruzza, L., D. Pantosti, D. Slejko, and G. Valensise (1997). Testing a new hybrid approach to seismic hazard assessment: An application to the Calabrian arc (southern Italy), *Nat. Hazards* **14,** 113–126.

Pettenati, F., L. Sirovich, and D. Sandron (2011). Rapid simulation of seismic intensities for civil protection purposes: Two recent cases in Italy, *Seismol. Res. Lett.* **82,** no. 3, 420–430, doi: 10.1785/gssrl.82.3.420.

Piatanesi, A., and S. Tinti (2002). Numerical modelling of the September 8, 1905 Calabrian (southern Italy) tsunami, *Geophys. J. Int.* **150,** 271–284, doi: 10.1046/j.1365-246X.2002.01700.x.

Pizzino, L., P. Burrato, F. Quattrocchi, and G. Valensise (2004). Geochemical signatures of large active faults: The example of the 5 February 1783, Calabrian earthquake (southern Italy), *J. Seismol.* **8,** no. 3, 363–380, doi: 10.1023/B:JOSE.0000038455.56343.e7.

Porfido, S., E. Esposito, C. Violante, F. Molisso, M. Sacchi, and E. Spiga (2011). *Earthquakes-Induced Environmental Effects in Coastal Area: Some Examples in Calabria and Sicily (Southern Italy)*, Marine Research at CNR, Dipartimento Terra e Ambiente, 1–12.

Postpischl, D. (1985). *Catalogo dei terremoti italiani dall'anno 1000 al 1980*, Consiglio Nazionale delle Ricerche, Progetto Finalizzato Geodinamica, Graficoop, Bologna, 239 pp. (in Italian).

Progetto AVI (2014). *Archivio frane—Sistema Informativo sulle Catastrofi Idrogeologiche*, IRPI—Istituto di Ricerca per la Protezione Idrogeologica del Consiglio Nazionale delle Ricerche, GNDCI—Gruppo Nazionale per la Difesa dalle Catastrofi Idrogeologiche del Consiglio Nazionale delle Ricerche (in Italian).

Progetto IFFI (2006). *Inventario dei Fenomeni Franosi in Italia*, ISPRA—Dipartimento Difesa del Suolo—Servizio Geologico d'Italia (in Italian).

Riuscetti, M., and R. Schick (1975). Earthquakes and tectonics in southern Italy, *Boll. Geof. Teor. Appl.* **17,** 59–78.

Rizzo, G. B. (1906). Sulla velocità di propagazione delle onde sismiche del terremoto della Calabria del giorno 8 Settembre 1905, *Mem. R. Accad. Sc. Torino* 2**,** no. 57, 42 pp. (in Italian).

Rosenbaum, G., M. Gasparon, F. P. Lucente, A. Peccerillo, and M. S. Miller (2008). Kinematics of slab tear faults during subduction segmentation and implications for Italian magmatism, *Tectonics* **27,** no. 2, TC2008, doi: 10.1029/2007TC002143.

Rovida, A., R. Camassi, P. Gasperini, and M. Stucchi (Editors) (2011). *CPTI11, la versione 2011 del Catalogo Parametrico dei Terremoti Italiani*, Milano, Bologna, doi: 10.6092/INGV.IT-CPTI11.

Sandron, D., and M. F. Loreto (2012). ISTEGE Project: Modeling of seismogenic sources, Istituto Nazionale di Oceanografia e Geofisica Sperimentale (OGS), *Internal Report 2011/37* (in Italian).

Sandron, D., P. Suhadolc, and G. Costa (2008). Source complexity effect on ground shaking scenarios, *Boll. Geof. Teor. Appl.* **49,** no. 2, 227–237.

Saraò, A., S. Das, and P. Suhadolc (1998). Effect of non-uniform station coverage on the inversion for earthquake rupture history for a Haskell-type source model, *J. Seismol.* **2,** 1–25.

Schweitzer, J., and W. H. K. Lee (2003). Old seismic bulletins to 1920: A collective heritage from early seismologists, in *International Handbook of Earthquake and Engineering Seismology, Part B*, W. H. K. Lee, H. Kanamori, P. C. Jennings, and C. Kisslinger (Editors), Academic Press, Amsterdam, 1665–1723.

Sieberg, A. (1930). Geologie der Erdbeben, *Handbuch der Geophysik* **2,** no. 4, 550–555.

Sirovich, L., F. Pettenati, F. Cavallini, and M. Bobbio (2002). Natural-neighbor isoseismals, *Bull. Seismol. Soc. Am.* **92,** 1933–1940.

Sommerville, P., K. Irikura, R. Graves, S. Sawada, D. Wald, N. Abrahamson, Y. Iwasaki, T. Kagawa, N. Smith, and A. Kowada (1999). Characterizing crustal earthquake slip models for the prediction of strong ground motion, *Seismol. Res. Lett.* **70,** no. 1, 59–80.

Suhadolc, P., D. Sandron, F. Fitzko, and G. Costa (2004). Seismic ground motion estimates for the **M** 6.1 earthquake of July 26, 1963 at Skopje, Republic of Macedonia, *Acta Geod. Geoph. Hung.* **39,** 319–326.

Tertulliani, A., and L. Cucci (2008). Fenomeni associati al terremoto della Calabria del 1905, *Quad. Geofisc.* **60,** 4–18 (in Italian).

Tertulliani, A., and L. Cucci (2009). Clues to the identification of a seismogenic source from environmental effects: The case of the 1905 Calabria (southern Italy) earthquake, *Nat. Hazards Earth Syst. Sci.* **9,** 1787–1803, doi: 10.5194/nhess-9-1787-2009.

Tiberi, L., G. Costa, and P. Suhadolc (2014). Source parameter estimates for some historical earthquakes in the southeastern Alps using ground shaking scenarios, *Boll. Geofis. Teor. Appl.* **5,** 641–664.

Tiberti, M. M., U. Fracassi, and G. Valensise (2006). Il quadro sismotettonico del grande terremoto del 1905, in *8 Settembre 1905, Terremoto in Calabria*, I. Guerra and A. Bavaglio (Editors), Università della Calabria, 181–205 (in Italian).

Tinti, S., and A. Maramai (1996). Catalogue of tsunamis generated in Italy and in Côte d'Azur, France: A step towards a unified catalogue of tsunamis in Europe, *Ann. Geofisc.* **39,** no. 6, 1253–1299.

Tortorici, G., M. Bianca, G. De Guidi, C. Monaco, and L. Tortorici (2003). Fault activity and marine terracing in the Capo Vaticano area (southern Calabria) during the Middle-Late Quaternary, *Quaternary Int.* **101/102,** 269–278, doi: 10.1016/S1040-6182(02)00107-6.

Valensise, G., and D. Pantosti (2001). The investigation of potential earthquake sources in peninsular Italy: A review, *J. Seismol.* **5,** no. 3, 287–306, doi: 10.1023/A:1011463223440.

Van Dijk, J. P. (1991). Basin dynamics and sequence stratigraphy in the Calabrian arc (central Mediterranean); Records and pathways of the Crotone basin, *Geol. Mijnbouw* **70,** 187–201.

Van Dijk, J. P. (1992). Late Neogene fore-arc basin evolution in the Calabrian arc (central Mediterranean); tectonic sequence stratigraphy and dynamic geohistory. With special reference to the geology of central Calabria, *Geol. Ultraiect.* **92,** 288.

Van Dijk, J. P., and P. J. J. Scheepers (1995). Neotectonic rotations in the Calabrian arc; implications for a Pliocene-recent geodynamic scenario for the central Mediterranean, *Earth Sci. Rev.* **39,** 207–246.

Van Dijk, J. P., M. Bello, G. P. Brancaleoni, G. Cantarella, V. Costa, A. Frixa, F. Golfetto, S. Merlini, M. Riva, S. Toricelli, C. Toscano, and A. Zerilli (2000). A new structural model for the northern sector of the Calabrian arc, *Tectonophysics* **324,** 267–320.

Wald, D. J., V. Quitoriano, T. H. Heaton, H. Kanamori, C. W. Scrivner, and C. B. Worden (1999). TriNet "ShakeMaps": Rapid generation of peak ground motion and intensity maps for earthquakes in southern California, *Earthq. Spectra* **15,** 537.

Wells, D., and K. Coppersmith (1994). New empirical relationship among magnitude, rupture length, rupture width, rupture area and surface displacement, *Bull. Seismol. Soc. Am.* **84,** 974–1002.

Wessel, P., and W. H. F. Smith (1998). New, improved version of Generic Mapping Tools released, *Eos Trans. AGU* **79,** no. 47, 579.

Westaway, R. (1992). Seismic moment summation for historical earthquakes in Italy: Tectonic implications, *J. Geophys. Res.* **97,** no. B11, 15,437–15,464.

Westaway, R. (1993). Quaternary uplift of southern Italy, *J. Geophys. Res.* **98,** no. B12, 741–772.

Yih-Min, W., T. Ta-liang, S. Tzay-Chyn, and H. Nai-Chi (2003). Relation between peak ground acceleration, peak ground velocity and intensity in Taiwan, *Bull. Seismol. Soc. Am.* **93,** no. 1, 386–396.

Istituto Nazionale di Oceanografia e Geofisica Sperimentale (OGS)
Borgo Grotta Gigante, 42C
34010 Sgonico, Trieste, Italy
dsandron@inogs.it
(D.S.)

Istituto di Scienze Marine-Consiglio Nazionale delle Ricerche (ISMAR-CNR)
Via P. Gobetti
101-40129 Bologna, Italy
(M.F.L.)

Istituto Nazionale di Geofisica e Vulcanologia
Via di Vigna Murata 605
00143 Rome, Italy
(U.F.)

Dipartimento di Matematica e Geoscienze
Università degli studi di Trieste
Via Weiss 4
34129 Trieste, Italy
(L.T.)

Manuscript received 18 February 2014